Pattern formation in reaction–diffusion systems on evolving surfaces

Hyundong Kim [a], Ana Yun [b], Sungha Yoon [a], Chaeyoung Lee [a], Jintae Park [a], Junseok Kim [a],*

[a] *Department of Mathematics, Korea University, Seoul 02841, Republic of Korea*
[b] *Buram high school, Seoul 01736, Republic of Korea*

ARTICLE INFO

ABSTRACT

In this paper, we propose an explicit time-stepping scheme for the pattern formation in reaction–diffusion systems on evolving surfaces. The proposed numerical method is based on a simple discretization scheme of Laplace–Beltrami operator over triangulated surface. On the static and evolving domains, we perform various numerical experiments for effect of domain growth and pattern formations. The computational results demonstrate that our proposed method can simulate pattern formation in reaction–diffusion systems on evolving surfaces. The actual zebra skin pattern and computational results are compared. In the computational results, we can observe different pattern formations on the evolving surface with specific rotation speed.

© 2020 Elsevier Ltd. All rights reserved.

1. Introduction

After Turing proposed the reaction–diffusion system to describe phenomena of morphogenesis [1], the reaction–diffusion systems have drawn significant interest. In the biological field, the reaction–diffusion systems may show the specific patterns including animal coat markings, formation of skin organs, pinning of diffusional patterns [2,3], and cell-division [4] depending on initial conditions, spatial scale, and geometry. To solve the reaction–diffusion systems which exhibit the pattern formation efficiently, the numerical scheme has been developed, like a work in [4]. Moreover, to consider the geometry, pattern formations on the curved surfaces have been studied with various numerical methods. The reaction–diffusion system on the surfaces was solved numerically using the finite element method in [5,6]. The modified Galerkin method was proposed to solve the reaction–diffusion equations on implicit surfaces [7]. A finite difference method has been used to solve the partial differential equations on the curved surfaces [8–10] where the closest point method in narrow band domain, or Laplace–Beltrami operator on triangulated surfaces is used. During the pattern development, growth of domain is an important factor for fundamental change [11,12]. Therefore, the pattern formation on the growing domains has been studied by many authors [13–15] including isotropic [3,16] and anisotropic growth [17]. The domain growth can be implemented to model the cortical folding pattern of the human brain [12].

In this paper, we shall study the pattern formation in the reaction–diffusion system on evolving surfaces with different initial conditions, as an extension of our previous study [18] which simulates the zebra skin pattern formation numerically

---

* Corresponding author.
E-mail addresses: rlagusehd@korea.ac.kr (H. Kim), cfdkim@korea.ac.kr (J. Kim).
URL: http://math.korea.ac.kr/~cfdkim (J. Kim).

on the static three-dimensional space. Especially, we focus on the formation of zebra striping patterns as our starting point to investigate generation of pattern on evolving surfaces. We propose an explicit time-stepping scheme for the pattern formation in reaction–diffusion systems on the growing two-dimensional (2D) space and evolving surfaces in the three-dimensional (3D) space. First, we validate the patterns are well formed in the two-dimensional static domain, then we shall perform to the numerical experiments by gradually expanding to static curved surfaces and evolving curved surfaces. The proposed numerical method is based on a simple discretized Laplace–Beltrami operator [19] to solve the Laplacian on the triangulated curved surface. Here, we use a finite difference method as the finite element method is difficult to implement and an implicit method is rather computationally costly [9]. Then we perform various numerical tests to demonstrate that our proposed method simulates the pattern formation in the reaction–diffusion system robustly on evolving surfaces.

This article is constructed as follows: We briefly introduce the mathematical model in Section 2. In Section 3, we present the numerical solutions in the two-dimensional space and on the curved surface. Based on the linear stability analysis, we investigate the growth mode of the mathematical model and we perform the numerical experiments on the static domain and evolving curved surface in Section 4. Finally, discussions are drawn in Section 5.

2. Mathematical model

To study of the pattern formation in the reaction–diffusion system on smooth closed surfaces $\mathcal{S}$ in $\mathbb{R}^3$, we consider the following reaction–diffusion systems:

$$
\begin{aligned}
\frac{\partial u}{\partial t} &= D_u \Delta_{\mathcal{S}} u + f(u, v) \\
\frac{\partial v}{\partial t} &= D_v \Delta_{\mathcal{S}} v + g(u, v)
\end{aligned}
\tag{1}
$$

where $u(\mathbf{x}, t)$ and $v(\mathbf{x}, t)$ are concentrations of an inhibitor and an activator at position $\mathbf{x} \in \mathcal{S}$ and time t, respectively. $f(u, v)$ and $g(u, v)$ are the reaction kinetics terms which typically are nonlinear functions. Here, D_u and D_v are the diffusion coefficients for u and v, respectively. Also, $\Delta_{\mathcal{S}}$ denotes the Laplace–Beltrami operator [20].

To perform numerical simulations of pattern formation on evolving surfaces, we take $f(u, v)$ and $g(u, v)$ of specific reaction kinetics form with quadratic and cubic terms [2]. The governing systems are derived from systems (1) in the following way. With a stationary uniform solution (u_s, v_s) given by the zeros of $f(u, v)$ and $g(u, v)$, the functions f and g are expanded by using a Taylor series around the stationary uniform solution without terms of higher order than cubic. Therefore, the governing systems have the following specific reaction–diffusion form with the homogeneous Neumann boundary condition:

$$
\begin{aligned}
\frac{\partial u}{\partial t} &= D\delta \Delta_{\mathcal{S}} u + \alpha u(1 - r_1 v^2) + v(1 - r_2 u), \\
\frac{\partial v}{\partial t} &= \delta \Delta_{\mathcal{S}} v + \beta v \left(1 + \frac{\alpha r_1}{\beta} uv \right) + u(\gamma + r_2 v),
\end{aligned}
\tag{2}
$$

where the quantity δ is the ratio of the diffusion coefficient for the two chemicals, r_1 and r_2 are the interaction parameters, D, α, β and γ are free parameters. It is known that spot or stripe patterns could be generated by the nonlinearity effect of quadratic and cubic interactions in systems (2), respectively [21,22]. These reaction–diffusion systems have been widely applied in the mathematical biology field, representatively such as in fish skin patterning [2], pattern formation on curved surface [23], generating pigment patterns on the leopard and the jaguar [24].

3. Numerical solution

3.1. Discretization of reaction–diffusion systems in the growing two-dimensional domain

We apply the explicit Euler method to solve the reaction–diffusion systems (1) in the growing two-dimensional domain. We conveniently denoted that $u_i^n = u(\mathbf{x}_i, n\Delta t)$ and $v_i^n = v(\mathbf{x}_i, n\Delta t)$, where Δt is the time step size. Here, we consider nonuniform mesh with different spatial step sizes h_i and h_j. i.e., $x_{i+1} = x_i + h_i$ for $x_0 = 0$, $i = 0, \ldots, N_{x-1}$, where N_x is the number of grid intervals and h_i is the grid spacing in x-direction. Likewise, $y_{j+1} = y_j + h_j$ for $y_0 = 0$, $j = 0, \ldots, N_{y-1}$, where N_y is the number of grid intervals and h_j is the grid spacing in y-direction. Let us consider the first and second derivatives with respect to x in 1D and it is defined analogously with respect to y.

$$
\begin{aligned}
\left(\frac{\partial u}{\partial x} \right)_i^n &= \frac{h_i}{h_{i-1}(h_{i-1} + h_i)} u_{i-1}^n + \frac{h_i - h_{i-1}}{h_{i-1} h_i} u_i^n + \frac{h_{i-1}}{h_i(h_{i-1} + h_i)} u_{i+1}^n, \\
\left(\frac{\partial^2 u}{\partial x^2} \right)_i^n &= \frac{2}{h_{i-1}(h_{i-1} + h_i)} u_{i-1}^n - \frac{2}{h_{i-1} h_i} u_i^n + \frac{2}{h_i(h_{i-1} + h_i)} u_{i+1}^n.
\end{aligned}
$$

Then, we have the discretized Laplacian Δ_d in the two-dimensional space

$$
\begin{aligned}
\Delta_d u_{ij}^n = {} & \frac{2}{h_{i-1}(h_{i-1}+h_i)} u_{i-1,j}^n - \frac{2}{h_{i-1}h_i} u_{ij}^n + \frac{2}{h_i(h_{i-1}+h_i)} u_{i+1,j}^n \\
& + \frac{2}{h_{j-1}(h_{j-1}+h_j)} u_{i,j-1}^n - \frac{2}{h_{j-1}h_j} u_{ij}^n + \frac{2}{h_j(h_{j-1}+h_j)} u_{i,j+1}^n.
\end{aligned}
$$

Therefore, the governing systems are discretized as

$$
\begin{aligned}
\frac{u_{ij}^{n+1} - u_{ij}^n}{\Delta t} &= D\delta \Delta_d u_{ij}^n + \alpha u_{ij}^n (1 - r_1(v_{ij}^n)^2) + v_{ij}^n(1 - r_2 u_{ij}^n), \\
\frac{v_{ij}^{n+1} - v_{ij}^n}{\Delta t} &= \delta \Delta_d v_{ij}^n + \beta v_{ij}^n \left(1 + \frac{\alpha r_1}{\beta} u_{ij}^n v_{ij}^n\right) + u_{ij}^n(\gamma + r_2 v_{ij}^n).
\end{aligned}
\tag{3}
$$

3.2. Discretization of Laplace–Beltrami operator on the curved surfaces

Now, we shall apply the simple discretization of Laplace–Beltrami operator [19,25] on the curved surfaces.

Let M be a triangular surface mesh of given surfaces $\mathcal{S}$ as shown in Fig. 1(a). With N points, the set $\{\mathbf{x}\}_{i=1}^N$ is called the surface vertex set of M. For each surface vertex $\mathbf{x}_i$ with index n, let us denote that $N_1(i) = \{i_1, i_2, \ldots, i_n\}$ is a set of surface vertex indices of one-ring neighbors with $i_1 = i_n$ as shown in Fig. 1(b). We simply denote by $u(\mathbf{x}_i) = u_i$, $v(\mathbf{x}_i) = v_i$, and T_j is a triangle consisting of vertices $\mathbf{x}_i$, $\mathbf{x}_{j_-}$ and $\mathbf{x}_j$. $A(\mathbf{x}_i)$ is the sum of areas of each triangle T_j encircling vertex $\mathbf{x}_i$ (see Fig. 1(d)) and it has the following form [19]:

$$
A(\mathbf{x}_i) = \sum_{j \in N(i)} \frac{\sqrt{\|\mathbf{x}_j - \mathbf{x}_i\|^2 \|\mathbf{x}_{j_+} - \mathbf{x}_i\|^2 - (\mathbf{x}_j - \mathbf{x}_i, \mathbf{x}_{j_+} - \mathbf{x}_i)^2}}{2}.
\tag{4}
$$

From curvature normal formula [26], we get the following discretization systems over the given surface $\mathcal{S}$ [20]:

$$
\begin{aligned}
\Delta_{\mathcal{S}} u_i &\approx \frac{3}{A(\mathbf{x}_i)} \sum_{j \in N(i)} \frac{\cot\theta_{ij} + \cot\theta_{ij_+}}{2}(u_j - u_i), \\
\Delta_{\mathcal{S}} v_i &\approx \frac{3}{A(\mathbf{x}_i)} \sum_{j \in N(i)} \frac{\cot\theta_{ij} + \cot\theta_{ij_+}}{2}(v_j - v_i),
\end{aligned}
\tag{5}
$$

where θ_{ij} and θ_{ij_+} are angles in triangles T_j and T_{j+}, respectively (see Fig. 1(c)).

Then, the governing system is discretized as

$$
\begin{aligned}
\frac{u_i^{n+1} - u_i^n}{\Delta t} &= D\delta \Delta_{\mathcal{S}} u_i^n + \alpha u_i^n(1 - r_1(v_i^n)^2) + v_i^n(1 - r_2 u_i^n), \\
\frac{v_i^{n+1} - v_i^n}{\Delta t} &= \delta \Delta_{\mathcal{S}} v_i^n + \beta v_i^n \left(1 + \frac{\alpha r_1}{\beta} u_i^n v_i^n\right) + u_i^n(\gamma + r_2 v_i^n).
\end{aligned}
\tag{6}
$$

4. Numerical results

4.1. Linear stability analysis in the static domain

We let $\gamma = -\alpha$ to have the unique equilibrium point $(\bar{u}, \bar{v}) = (0, 0)$ throughout this paper. If we linearize systems (2) at the unique equilibrium point $(\bar{u}, \bar{v}) = (0, 0)$, we have

$$
\begin{aligned}
\frac{\partial u}{\partial t}(\mathbf{x}, t) &= D\delta \Delta u(\mathbf{x}, t) + \alpha u(\mathbf{x}, t) + v(\mathbf{x}, t), \\
\frac{\partial v}{\partial t}(\mathbf{x}, t) &= \delta \Delta v(\mathbf{x}, t) + \beta v(\mathbf{x}, t) + \gamma u(\mathbf{x}, t).
\end{aligned}
\tag{7}
$$

Let us assume the solutions to the linearized systems (7) have the following form:

$$
u(x, y, t) = F(t)\cos(kx), \quad v(x, y, t) = G(t)\cos(kx).
\tag{8}
$$

After substituting Eq. (8) into systems (7), we obtain

$$
\begin{pmatrix} F(t) \\ G(t) \end{pmatrix}' = A \begin{pmatrix} F(t) \\ G(t) \end{pmatrix}, \quad A = \begin{pmatrix} -k^2 D\delta + \alpha & 1 \\ \gamma & -k^2\delta + \beta \end{pmatrix},
\tag{9}
$$

where $'$ is the temporal derivative. The characteristic polynomial is

$$
\lambda^2 + (-\alpha - \beta + \delta k^2(1+D))\lambda + D\delta^2 k^4 - (\alpha + \beta D)\delta k^2 + \alpha\beta - \gamma = 0.
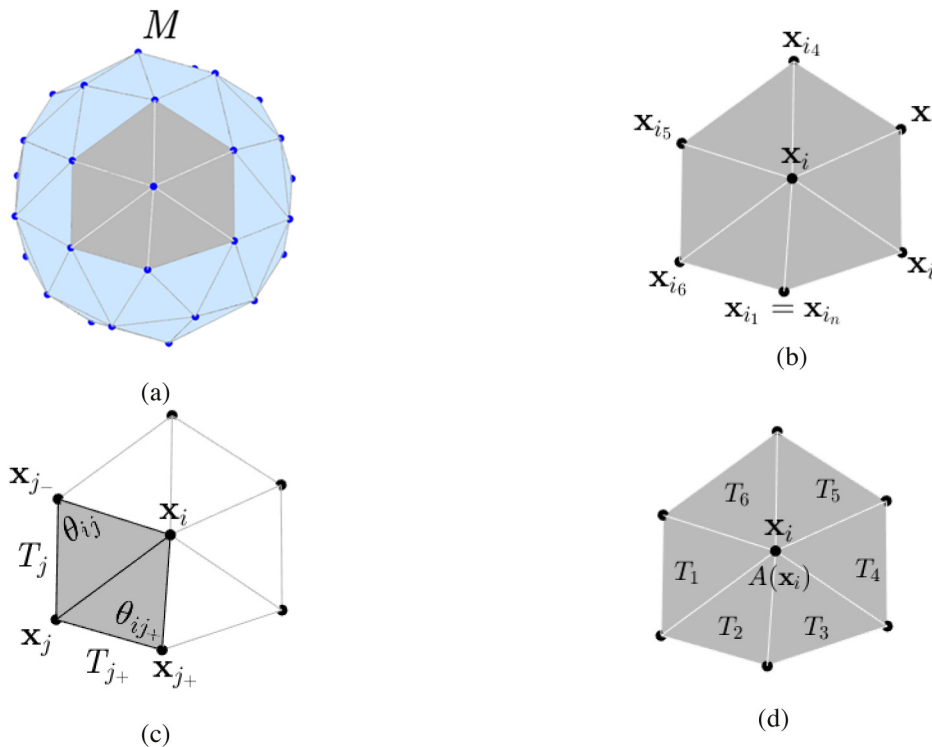\tag{10}
$$

Fig. 1. Schematic illustrations of (a) triangulation of surfaces, (b) the surface vertices set of one-ring neighbors of $\mathbf{x}_i$ with $i_1 = i_n$, (c) triangles T_j and T_{j_+} with the angles θ_{ij} and θ_{ij_+}, and (d) area $A(\mathbf{x}_i)$ at vertex $\mathbf{x}_i$.

Therefore, the eigenvalues of A are

$$\lambda_1 = \frac{1}{2}\left(\alpha + \beta - \delta k^2(1+D) - B\right), \quad \lambda_2 = \frac{1}{2}\left(\alpha + \beta - \delta k^2(1+D) + B\right), \tag{11}$$

where $B = \sqrt{(\alpha - \beta)^2 + 4\gamma + 2(\alpha - \beta)(1-D)\delta k^2 + \delta^2(D-1)^2 k^4}$.

The corresponding eigenvectors are

$$X_1 = \left(\frac{\alpha - \beta + (1-D)\delta k^2 - B}{2\gamma}, \ 1\right)^T, \tag{12}$$

$$X_2 = \left(\frac{\alpha - \beta + (1-D)\delta k^2 + B}{2\gamma}, \ 1\right)^T. \tag{13}$$

The solution to the system of ODEs (9) is given by

$$\begin{pmatrix} F(t) \\ G(t) \end{pmatrix} = C_1 X_1 e^{\lambda_1 t} + C_2 X_2 e^{\lambda_2 t}, \tag{14}$$

where

$$\begin{pmatrix} C_1 \\ C_2 \end{pmatrix} = (X_1 \ X_2)^{-1} \begin{pmatrix} f(0) \\ g(0) \end{pmatrix}.$$

Fig. 2(a) shows the eigenvalues λ_1 (solid line) and λ_2 (dashed line) of the linearized system (11) with the parameter sets $D = 0.516, \delta = 2, \alpha = 0.899$, and $\beta = -0.95$. Let us consider the initial conditions:

$$u(x, y, 0) = 0.01\cos(kx), \quad v(x, y, 0) = 0.01\cos(kx). \tag{15}$$

Then, we compare the solutions of ODEs $F(t)$ and $G(t)$ in (14) to numerical solutions. In Fig. 2, (b) and (c) are the numerical results with the linear stability solution (14) for $k = 0.7$, and $k = 1.1$, respectively. Here, $f_{max}(t)$ (solid line) and $g_{max}(t)$ (dotted line) are analytic solutions for u and v, respectively. $F_{max}(t)$ (circles) which is the maxima of the numerical solution for u and $G_{max}(t)$ (squares) which is the maxima of the numerical solution for v. With chosen initial conditions, we observe that the numerical solutions agree well with $f_{max}(t)$ and $g_{max}(t)$.
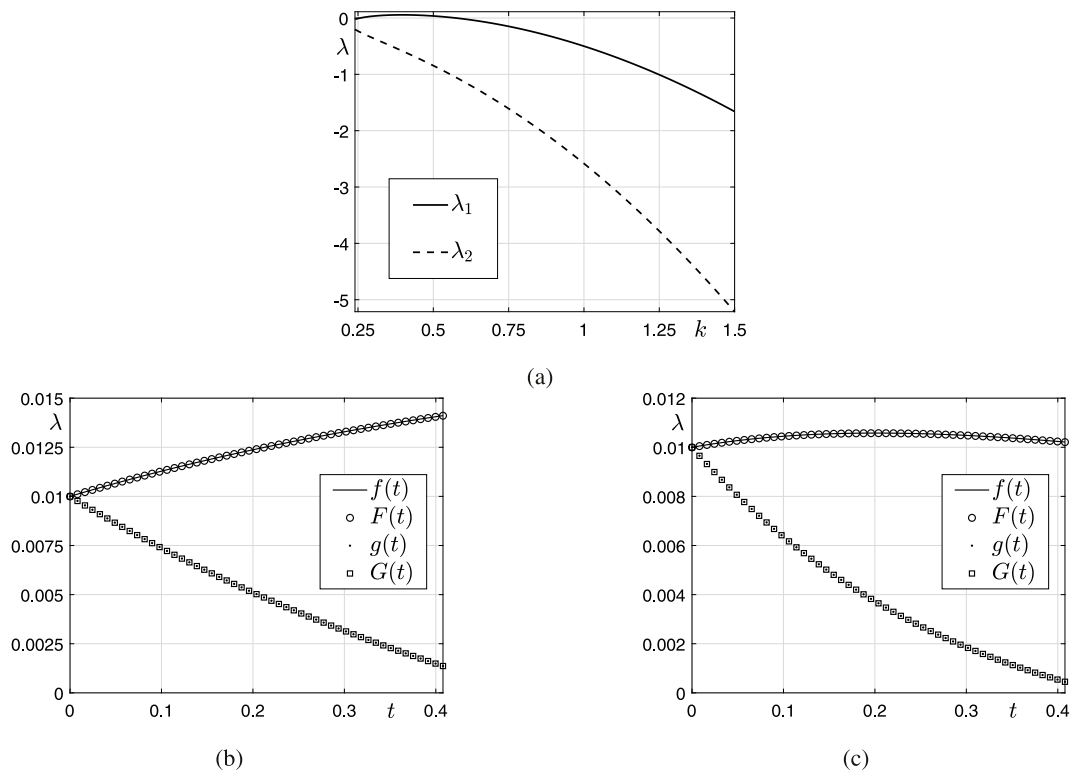
(a)

(b)

(c)

Fig. 2. (a) Eigenvalues λ_1 (solid line) and λ_2 (dashed line) of the linearized system (9) with $D = 0.516$, $\delta = 2$, $\alpha = 0.899$, and $\beta = -0.95$. (b) and (c) are the numerical results with the linear stability solution (14) for $k = 0.7$ and $k = 1.1$, respectively. Here, $f_{max}(t)$ (solid line) is the analytic solution for u and $g_{max}(t)$ (dotted line) is the analytic solution for v. $F_{max}(t)$ (circles) and $G_{max}(t)$ (squares) are the maxima of the numerical solutions for u and v, respectively.

4.2. Effect of domain growth

4.2.1. Effect of domain growth in the two-dimensional space

Based on the growing mode, we shall implement the effect of the growing two-dimensional domain. First, we perform numerical experiments on the nonuniformly growing two-dimensional domain. The parameter set is chosen as $D = 0.516$, $\delta = 2$, $\alpha = 0.899$, $\beta = -0.95$, $r_1 = 3.5$, and $r_2 = 0$, where δ is scaled as 2 on the growing two-dimensional domain. With the initial conditions $u(x, y, 0) = 0.1 \cos(kx)$ and $v(x, y, 0) = 0.1 \cos(kx)$, we simulate the profile of v with respect to growing in the x-direction as shown in Fig. 3. Here, we set $k = 1.1$, on the domain $[0, 50\pi/k] \times [0, 5\pi/k]$, $N_x = 200$, $N_y = 20$, $h = \pi/(4k)$ and $\Delta t = 0.0025h^2$. With chosen parameter set and initial conditions, we can observe sequentially stretching stripe shapes in the x-direction, by the effect of domain growth.

Fig. 4 shows the snapshots at $t = 0$, $500\Delta t$, $1000\Delta t$ from left to right with the initial conditions $u(x, y, 0) = 0.1 \cos(k\sqrt{x^2 + y^2})$ and $v(x, y, 0) = 0.1 \cos(k\sqrt{x^2 + y^2})$. The parameter set is taken as $D = 0.516$, $\delta = 2$, $\alpha = 0.899$, $\beta = -0.95$, $r_1 = 3.5$ and $r_2 = 0$. Here, we set $k = 1.1$, on the domain $[0, 30\pi/k] \times [0, 30\pi/k]$, $N_x = N_y = 200$, $h = \pi/(4k)$ and $\Delta t = 0.0025h^2$. As shown in Fig. 4, we can observe that curved lines are sequentially changing flat lines by the domain growth in the x-, y-directions.

4.2.2. Effect of the domain growth on evolving curved surfaces

Now, we numerically investigate different type of the zebra skin patterns as shown in Fig. 5. Zebra skin patterns on the neck and legs show almost regular parallel stripes, however on the torso, patterns show stretched, split and demagnified stripes that are not regular as shown in Fig. 5(a). Also, in Fig. 5(b), we can see that the brightness of the zebra skin pattern is different. This happens when zebra grows up, and we shall consider observed patterns in the numerical simulations.

The evolving process of curved surfaces which having sphere as the initial state is schematically depicted in Fig. 6. Set $p(t) = (x(t), y(t), z(t))$ and let s be a scale parameter and c be a some constant. For $x(t) < 0$, we translate $p(t)$ to $p(t + \Delta t) = p(t) + s\Delta t(cx(t), y(t), z(t))$. Otherwise, we rotationally translate $p(t)$ to $p(t + \Delta t) = p(t) + s\Delta t\left((cx(t), y(t), z(t)) + x(t)\left((z(t), 0, -x(t)) - l\right)\right)$ if $x(t) \geq 0$. As shown in Fig. 6, $\mu = (-R, 0, 0)$ and $v = (x, y, z)$ are points on the surface. The angle θ is calculated using μ and v, and then we define $L = R\theta$ which is used to determine an initial value in each point. In the numerical experiments on evolving surfaces, we take $R = 100$, $c = 30$ and $l = (-75, 0, 0)$.
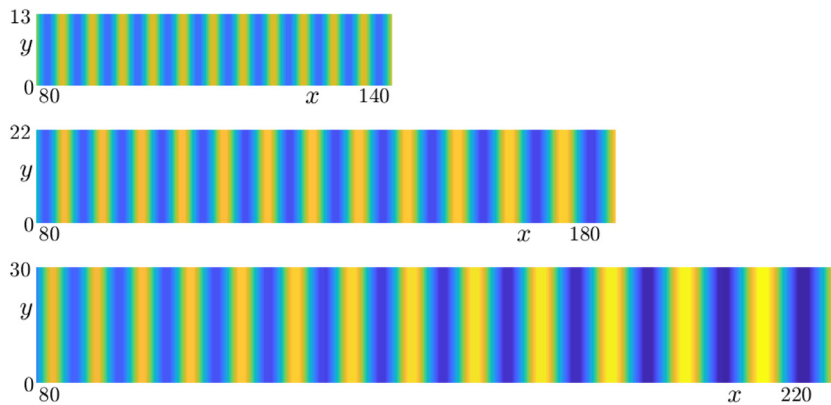
Fig. 3. Effect of the growing two-dimensional domain in the x-direction at $t = 0$, $500\Delta t$, $1000\Delta t$ from top to bottom, respectively.
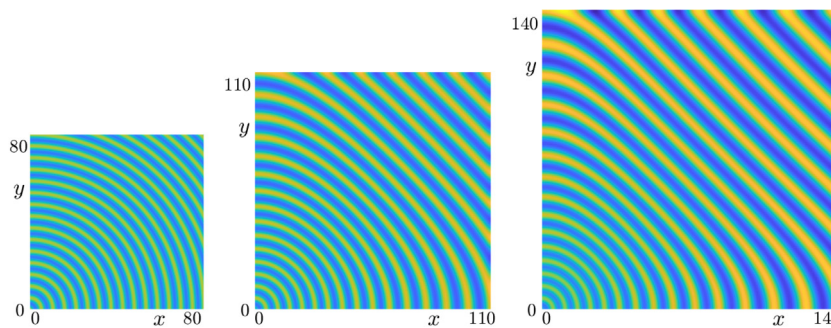

Fig. 4. Effect of the growing two-dimensional domain at $t = 0$, $500\Delta t$, $1000\Delta t$ from left to right, respectively.
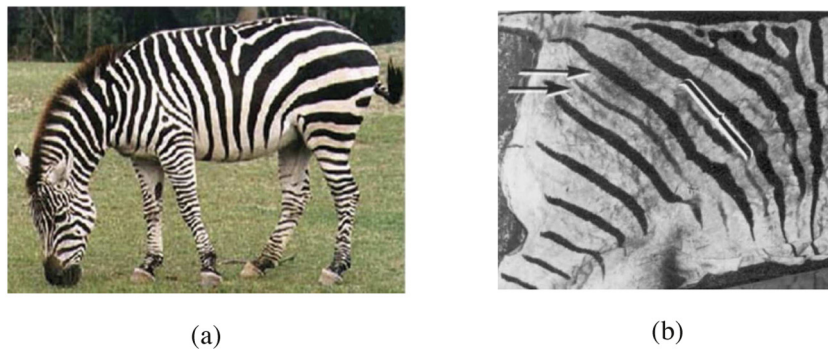

Fig. 5. Skin pattern on a zebra. Reprinted from (a) Grzybowski and Campbell [27] with permission from Elsevier, and from (b) Jonathan [28] with permission from John Wiley and Sons.

Note that $\bar{a} - \mathrm{p}$ is a vector which is orthogonal to the projection of $\mathrm{p} - a$ onto xz-plane, represented by $(z(t), 0, -x(t)) - l$ as above. Therefore, l is just normal to a on xz-plane.

From now on, we shall observe how effect of domain growth on evolving curved surface which having a sphere as the initial state, varies with rotation speed. In Fig. 7(a), the initial conditions are set to $u(x, y, z, 0) = 0.5\cos(30L)$ and $v(x, y, z, 0) = -0.25\cos(30L)$. The parameters used are $\Delta t = 0.025$, $D = 0.516$, $\delta = 3$, $\alpha = 0.899$, $\beta = -0.95$, and $\gamma = -\alpha$. By adding a condition that accelerates the rotation speed 1.5 times more after a certain number of iterations, in numerical simulations following the rules described above, we were able to observe the effect of domain growth such as stretching stripe shape, and splitting stripe shape, and then we can observe different stretching shapes, splitting shapes, and brightness with respect to different rotation speeds at the same shape, as shown in Fig. 7. First row of Fig. 7 has original rotation speed, and second row has 1.5 times rotation speed on evolving curved surface.
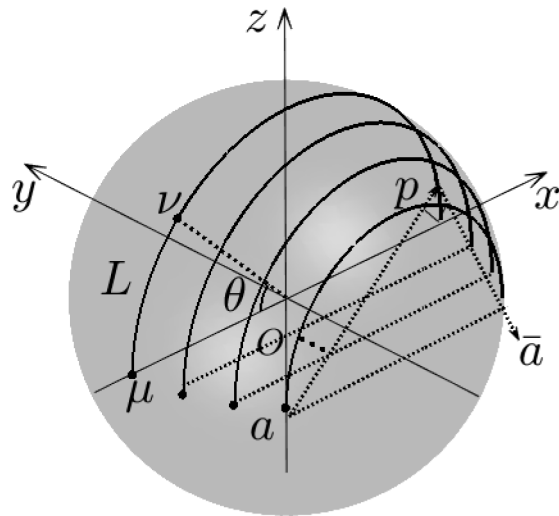
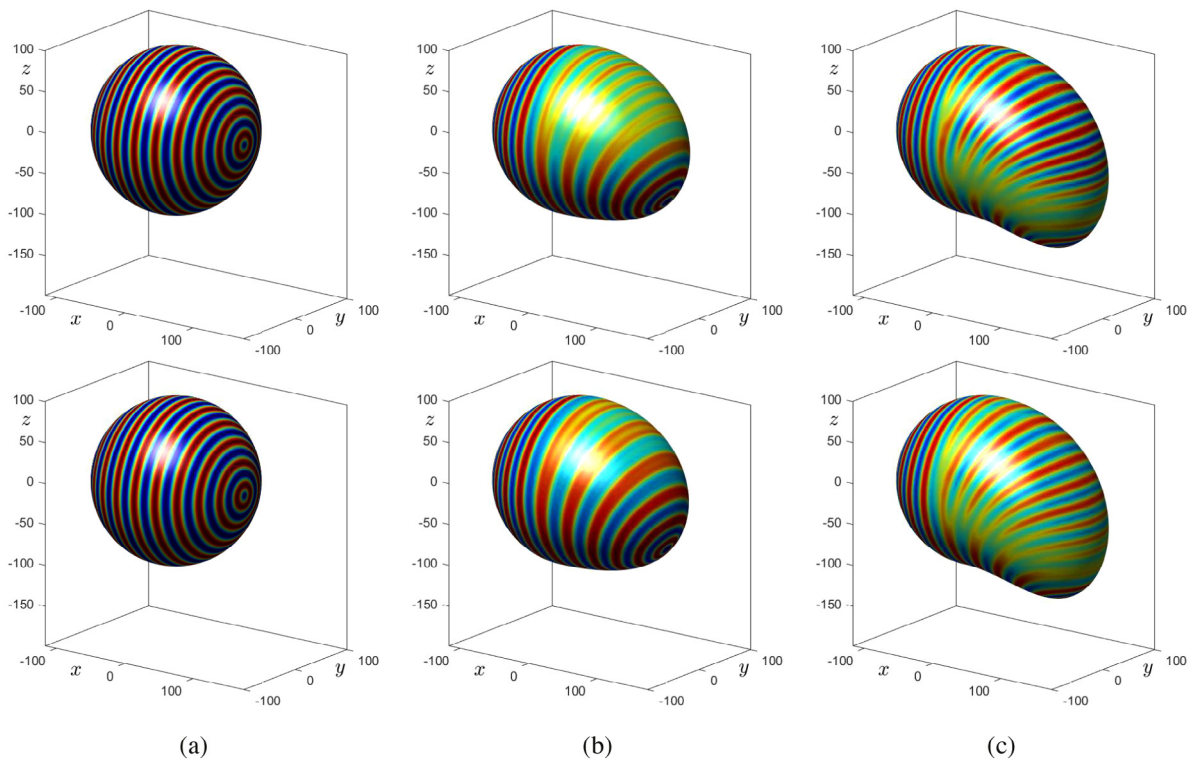**Fig. 6.** Schematic representation of the evolving of curved surfaces.

Fig. 7. From top to bottom, effect of domain growth on evolving curved surface with original and 1.5 times rotation speed at (a) $t = 0$, (b) $t = 65, 50$ and (c) $t = 100, 75$, respectively.

4.3. Pattern formation

4.3.1. Pattern formation on static curved surface

We perform the pattern formation on a curved surface $\mathcal{S}$. We investigate a phase separation of random initial condition on sphere as shown in Fig. 8. We used the triangular surface mesh to represent a sphere. Here, radius of sphere $R = 100$
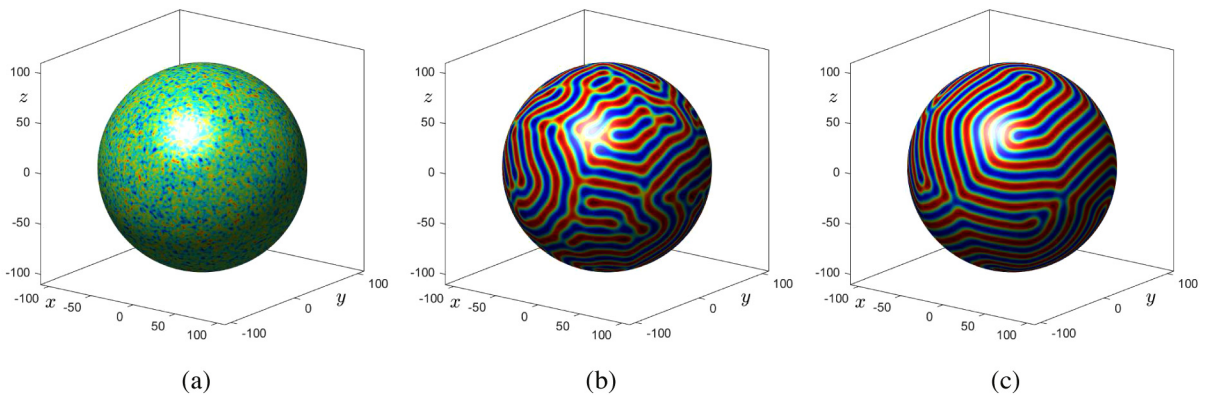
Fig. 8. Pattern formation in the reaction–diffusion systems on the static sphere at (a) $t = 0$, (b) $t = 500$, and (c) $t = 10000$.
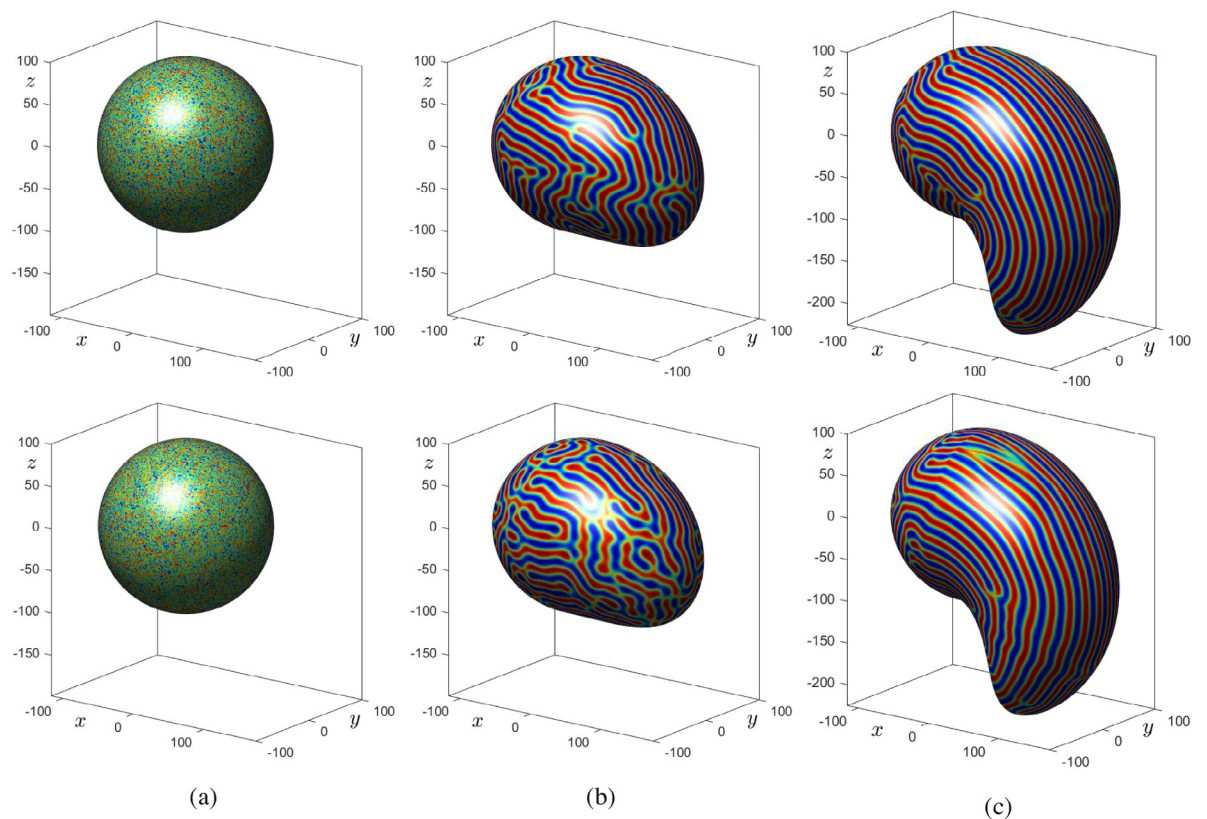

Fig. 9. From top to bottom, pattern formation in the reaction–diffusion systems on evolving curved surface with 0.1 times and 0.5 times rotation speed at (a) $t = 0$, (b) $t = 1050, 210$ and (c) $t = 3500, 700$, respectively.

is used. Furthermore, the parameters to the 3D extension of systems (3) are adopted as follows: $\Delta t = 0.1$, $D = 0.516$, $\delta = 3$, $\alpha = 0.899$, $\beta = -0.95$, and $\gamma = -\alpha$. In Fig. 8(a), the initial condition is given by $u(x, y, z, 0) = \text{rand}(x, y, z)$ and $v(x, y, z, 0) = \text{rand}(x, y, z)$, where $\text{rand}(x, y, z)$ denotes random number between 0 and 1. We can observe the pattern formation of reaction–diffusion systems at $t = 500$ in Fig. 8(b). In Fig. 8(c), the value of v at the edges of triangular patches is numerically in the range between -0.2743 and 0.2665, and we could observe that labyrinth-type pattern formations on the static sphere.

4.3.2. Pattern formation on evolving curved surface

Finally, we perform pattern formations on evolving curved surface which having sphere as the initial state. The initial conditions are set to $u(x, y, z, 0) = 2\text{rand}(x, y, z) - 1$ and $v(x, y, z, 0) = 2\text{rand}(x, y, z) - 1$, where $\text{rand}(x, y, z)$ denotes

random number between 0 and 1, as shown in Fig. 9. The parameters used are $\Delta t = 0.035$, $D = 0.516$, $\delta = 3$, $\alpha = 0.899$, $\beta = -0.95$, and $\gamma = -\alpha$. First row of Fig. 9 has 0.1 times rotation speed, and second row has 0.5 times rotation speed on evolving curved surface. As shown in temporal evolutions from Fig. 9(b) to (c), it can be seen that patterns are generated along rotational directions and the curvatures. Furthermore, splitting pattern formation seen in Fig. 7 could also be observed in the second row of Fig. 9(c). This splitting pattern formation cannot be found in the first row of Fig. 9(c). Therefore, we can see that the splitting pattern formation is depending on rotation speeds.

5. Discussions

In this article, we considered an explicit time-stepping scheme for pattern formation in reaction–diffusion systems on evolving surfaces. The proposed numerical method is based on a simple discretization scheme of Laplace–Beltrami operator over triangulated surface. We performed various numerical experiments and presented the computational results to demonstrate that our proposed method can simulate pattern formation in reaction–diffusion systems on evolving surfaces. The actual zebra skin pattern on the body part for each different growth condition as shown in Fig. 5 was compared with the effect of domain growth in the reaction–diffusion systems on the evolving surface with respect to the different rotation speeds as shown in Fig. 7. In future work, we shall study the pattern formations on the evolving surfaces with time dependent spectrum of Laplace–Beltrami operator, that can compare actual pattern formations.

CRediT authorship contribution statement

Hyundong Kim: Methodology, Software, Validation, Formal analysis, Investigation, Data curation, Writing - original draft, Writing - review & editing, Visualization, Project administration. **Ana Yun:** Software, Validation, Investigation, Writing - original draft, Writing - review & editing, Visualization. **Sungha Yoon:** Methodology, Software, Validation, Investigation, Writing - original draft, Visualization. **Chaeyoung Lee:** Investigation, Visualization, Writing - original draft, Writing - review & editing. **Jintae Park:** Software, Investigation, Writing - original draft. **Junseok Kim:** Conceptualization, Methodology, Software, Investigation, Formal analysis, Writing - original draft, Writing - review & editing, Supervision, Project administration, Funding acquisition.

References

[1] A.M. Turing, The chemical basis of morphogenesis, Bull. Math. Biol. 52 (1) (1990) 153–197.
[2] R.A. Barrio, C. Varea, J.L. Aragon, P.K. Maini, A two-dimensional numerical study of spatial pattern formation in interacting turing systems, Bull. Math. Biol. 61 (3) (1999) 483–505.
[3] E.J. Crampin, E.A. Gaffney, P.K. Maini, Reaction and diffusion on growing domains: scenarios for robust pattern formation, Bull. Math. Biol. 61 (6) (1999) 1093–1120.
[4] O.S. Iyiola, B.A. Wade, Exponential integrator methods for systems of non-linear space-fractional models with super-diffusion processes in pattern formation, Comput. Math. Appl. 75 (10) (2018) 3719–3736.
[5] D. Lacitignola, B. Bozzini, M. Frittelli, I. Sgura, Turing pattern formation on the sphere for a morphochemical reaction–diffusion model for electrodeposition, Commun. Nonlinear Sci. Numer. Simul. 48 (2017) 484–508.
[6] G. Dziuk, C.M. Elliott, Finite element methods for surface PDEs, Acta Numer. 22 (2013) 289–396.
[7] X. Xiao, K. Wang, X. Feng, A lifted local Galerkin method for solving the reaction–diffusion equations on implicit surfaces, Comput. Phys. Comm. 231 (2018) 107–113.
[8] H.G. Lee, J. Kim, A simple and efficient finite difference method for the phase-field crystal equation on curved surfaces, Comput. Math. Appl. Mech. Engrg. 307 (2016) 32–43.
[9] Y. Li, J. Kim, N. Wang, An unconditionally energy-stable second-order time-accurate scheme for the cahn–hilliard equation on surfaces, Commun. Nonlinear Sci. Numer. Simul. 53 (2017) 213–227.
[10] Y. Li, X. Qi, J. Kim, Direct discretization method for the cahn–hilliard equation on an evolving surface, J. Sci. Comput. 77 (2) (2018) 1147–1163.
[11] P.K. Maini, T.E. Woolley, R.E. Baker, E.A. Gaffney, S.S. Lee, Turing's model for biological pattern formation and the robustness problem, Interface Focus 2 (2012) 487–496.
[12] G. Toole, M.K. Hurdal, Turing models of cortical folding on exponentially and logistically growing domains, Comput. Math. Appl. 66 (9) (2013) 1627–1642.
[13] K.J. Painter, P.K. Maini, H.G. Othmer, Stripe formation in juvenile pomacanthus explained by a generalized turing mechanism with chemotaxis, Proc. Natl. Acad. Sci. 96 (10) (1999) 5549–5554.
[14] E.J. Crampin, W.W. Hackborn, P.K. Maini, Pattern formation in reaction–diffusion models with nonuniform domain growth, Bull. Math. Biol. 64 (4) (2002) 747–769.

[15] T. Miura, K. Shiota, G. Morriss-Kay, P.K. Maini, Mixed-mode pattern in doublefoot mutant mouse limb-turing reaction–diffusion model on a growing domain during limb development, J. Theoret. Biol. 240 (4) (2006) 562–573.
[16] F. Sánchez-Garduño, A.L. Krause, J.A. Castillo, P. Padilla, Turing—Hopf patterns on growing domains: the torus and the sphere, J. Theoret. Biol. 481 (2019) 136–150.
[17] A.L. Krause, M.A. Ellis, R.A. Van Gorder, Influence of curvature, growth, and anisotropy on the evolution of turing patterns on growing manifolds, Bull. Math. Biol. 81 (2019) 759–799.
[18] D. Jeong, Y. Li, Y. Choi, M. Yoo, D. Kang, J. Park, J. Choi, J. Kim, Numerical simulation of the zebra pattern formation on a three-dimensional model, Physica A 475 (2017) 106–116.
[19] G. Xu, Discrete Laplace–Beltrami operators and their convergence, Comput. Aided Geom. Design 21 (8) (2004) 767–784.
[20] G. Xu, Convergence of discrete Laplace–Beltrami operators over surfaces, Comput. Math. Appl. 48 (3) (2004) 347–360.
[21] B. Ermentrout, Stripes or spots? Nonlinear effects in bifurcation of reaction—diffusion equations on the square, Proc. R. Soc. Lond. Ser. A Math. Phys. Sci. 434 (1991) 413–417.
[22] B.N. Nagorcka, J.R. Mooney, From stripes to spots: prepatterns which can be produced in the skin by a reaction–diffusion system, Math. Med. Biol. 9 (4) (1992) 249–267.
[23] C. Varea, J.L. Aragon, R.A. Barrio, Turing patterns on a sphere, Phys. Rev. E 60 (4) (1999) 4588.
[24] R.T. Liu, S.S. Liaw, P.K. Maini, Two-stage turing model for generating pigment patterns on the leopard and the jaguar, Phys. Rev. E 74 (1) (2006) 011914.
[25] M. Desbrun, M. Meyer, P. Schröder, A.H. Barr, Implicit fairing of irregular meshes using diffusion and curvature flow, in: SIGGRAPH '99: Proceedings of the 26th Annual Conference on Computer Graphics and Interactive Techniques, 1999, pp. 317–324.
[26] M. Meyer, M. Desbrun, P. Schröder, A.H. Barr, Discrete differential-geometry operators for triangulated 2-manifolds, Vis. Math. 3 (2003) 35–57.
[27] B.A. Grzybowski, C.J. Campbell, Fabrication using 'programmed' reactions, Mater. Today 10 (6) (2007) 38–46.
[28] B.B. Jonathan, A unity underlying the different zebra striping patterns, J. Zool. 183 (4) (1977) 527–539.